Advanced Synchronization Control for Inverters Parallel Operation in Microgrids Using Coupled Hopf Oscillators

Mingshen Li, Baoze Wei, Jose Matas, Josep Maria Guerrero, and Juan Carlos Vasquez

***Abstract*—A simple high-performance decentralized controller based on Hopf oscillator is proposed for three-phase parallel voltage source inverter (VSI) in islanded Microgrid. In αβ frame, the oscillators equations corresponding output current and common bus voltage as feedbacks are designed according to coupled oscillator synchronization properties. The enough common bus information is considered to realize external synchronization, and the current feedback is to achieve internal synchronization between VSIs. Then, the controller employs Hopf evolution dynamics to integrate their both. Therefore, a larger phase error can be eliminated when additional inverter connects, and the pre-synchronization item is proposed to be close to synchronize with the operational inverters. In addition, an integrated small-signal states pace based on averaged model for two parallel VSIs is developed, and the root locus shows the large stability margin and low sensitivity of parameters. Simulation and experiment results verified the effectiveness of the proposed method in aspects of the fast dynamics response and precise current sharing performance.**

***Index Terms*—Current sharing, Hopf oscillator control, microgrid, paralleled three-phase inverters, synchronization.**

I. Introduction

POWER converters as the interfaces between sources and utility grid, play the important roles in microgrid structures, which have the functions such as converting power, stabilizing the output current or voltage, improving power quality and optimizing the power operation etc [1], [2]. The intrinsic quality of microgrid is the parallel operation of converters, synchronization and power sharing turn to the key objectives for microgrid control. The most used decentrulized control method for inverters in islanding microgrids is droop control, and the well known method requires no communication and is inspired by the synchrous generator in traditional grid. Droop control is a method which shows a linear droop characteristic between inverter frequency and voltage amplitude and the active and reactive power output, respectively [3]–[6]. However, droop control highlights some weakness: slow transient response caused by low pass filter (LPF), affected largely by the line impedance, and inaccurate power sharing. To occur these drawbacks, a series of improved droop methods are mainly divided to decoupled power control [7]–[9], virtual impedance method [10], [11], constructed and compensated methods [12], [13]. These various approaches are according to the droop characteristic control in essence. Another ideas for decentralized control is the voltage-current droop strategies. In [14], a synchronous-reference frame virtual impedance loop based controller was proposed to conquer above mentioned, but the applied phase-locked-loop (PLL) will limit the control bandwidth and the virtual impedance is complex to design.

Recently, a decentralized method named virtual oscillator control (VOC) have been carried out in [15]–[18], which is motived by the weakly coupled oscillator synchronization property. To compare with droop control, this method highlights the advantages: faster transient response, independency to loads and flexibility operation to line impedance. However, the deadzone and Van der Pol are typical harmonics oscillators which require a certain condition to get the ideal sinusoidal reference, and appromimate limit circle may introduce the additional harmonics in voltage reference. In addition, the initial states will affect the evolution speed from startup to steady state. In order to improve the oscillator controller, Hopf oscillator was applied into single phase inverters [19], which presents the faster response, the better robustness, and the firm limit cycle to improve power quality.

In order to cope with the issues of the previous decentralized controller, a simple and fast Hopf oscillator controller combined external and internal synchronization is proposed for three-phase parallel islanding inverters. The main contributions of this paper are listed as: 1) provide the advanced synchronization ability including phase locking with AC bus and current sharing instead of using traditional PLL and power droop calculation; 2) presents the averaged model to contribute the nonlinear droop and ascend characteristic analysis; 3) investigate the dynamics and sensitivity of system by using small signal model; 4) validates the effectiveness of proposed controller to compare with VOC and droop control in simulation, and experiments under several operation cases.

The rest of paper is organized as follows. In section II, the

Manuscript received July 16, 2020; revised September 2, 2020; accepted September 11, 2020. Date of publication September 30, 2020; date of current version September 23, 2020. This work was supported in part by Distributed Converter and Microgrid Advanced Control Algorithm from Huawei Cooperation Project under Grant YBN2018085257, and in part by a Villum Investigator Grant Center for Research on Microgrid under Grant 25920 from The Villum Fonden.

M. Li , B. Wei, J. M. Guerrero, and J. C. Vasquez are with the Dept. of Energy Technology, Aalborg University, 9220 Aalborg, Denmark (e-mail: msh@et.aau.dk; ygu@et.aau.dk; joz@et.aau.dk; juq@et.aau.dk).

J. Matas is with the Dept. of Electronic Engineering, Polytechnic University of Catalonia, 08800 Barcelona, Spain (e-mail: jose.matas@upc.edu).

Digital Object Identifier 10.24295/CPSSTPEA.2020.00019

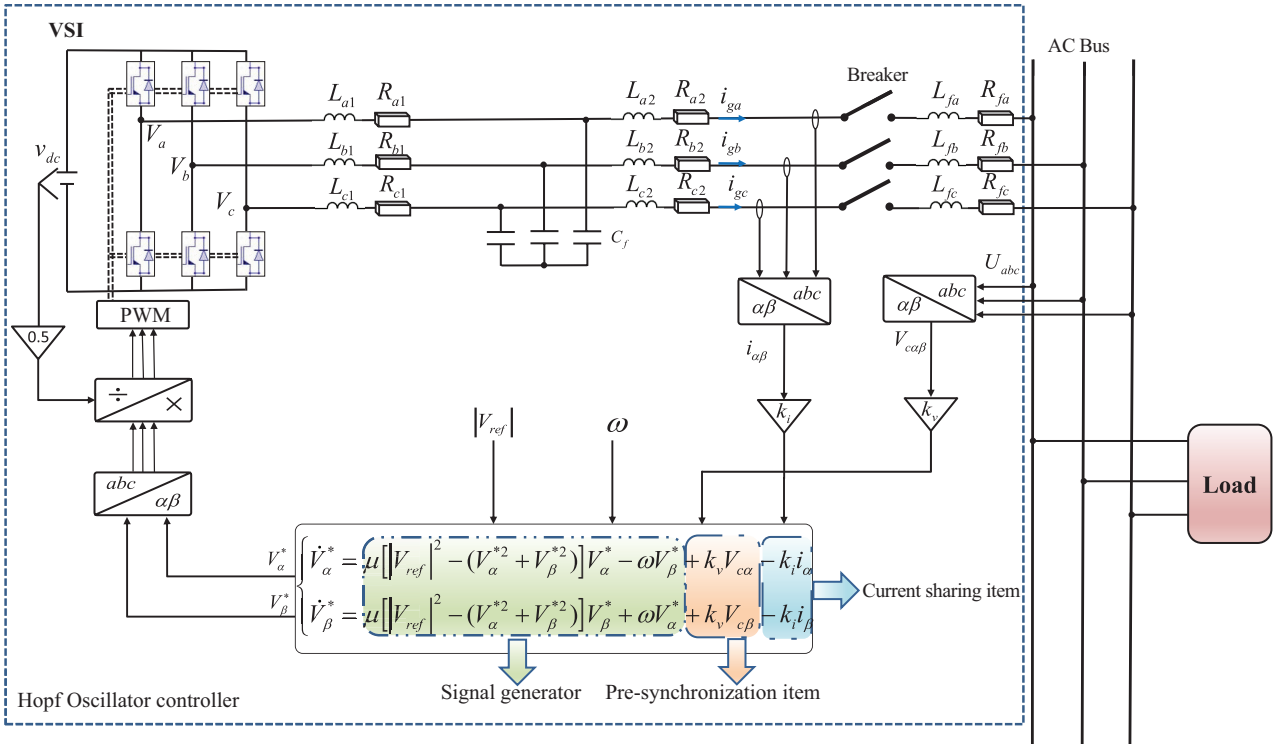

Fig. 1. Implementation of the proposed controller for three-phase islanded VSIs.

Hopf oscillator controller implementation and averaged model are presented, and key parameters are designed in details. Section III demonstrates the small signal stability analysis with considering the line impedance and key parameters. Section IV show the simulation results comparing with VOC and droop control. In Section V, the experiment validation of the proposed method under several cases are given. Finally, Section VI shows the conclusions of this study.

II. Proposed Contoller Implementation and Parameter Desigm

In this section, the proposed Hopf oscillator controller is introduced to describe the three-phase paralleled system, and the averaged model is derived for analyzing the controller properties. In addition, the parameters selection is discussed based on the nonlinear droop relationship of averaged model.

A. Controller Implementation

A Hopf type oscillator is able to generate a circular limit cycle and it has improved dynamics compared to Van der Pol oscillator. Considering the voltage and current are three phase, the controller should be designed in stationary reference frame for the natural orthogonal output of Hopf oscillator. Thus, the controller is proposed as following equations:

$$\begin{cases} \dot{V}_\alpha^* = \mu\left(|V_{\text{ref}}|^2 - V_\alpha^{*2} - V_\beta^{*2}\right)V_\alpha^* - \omega V_\beta^* + k_v V_{c\alpha} - k_i i_\alpha \\ \dot{V}_\beta^* = \mu\left(|V_{\text{ref}}|^2 - V_\alpha^{*2} - V_\beta^{*2}\right)V_\beta^* + \omega V_\alpha^* + k_v V_{c\beta} - k_i i_\beta \end{cases} \quad (1)$$

where $V_{c\alpha\beta}$ are the measurement voltage components of common bus in $\alpha\beta$-frame, $i_{\alpha\beta}$ are the VSI output current components in $\alpha\beta$-frame, $V_{\alpha\beta}^*$ are the voltage references that are generated by Hopf oscillator. Meanwhile, k_v and k_i is the voltage and current gain, respectively, and μ is the damping coefficient that affects the time transient response speed of the oscillator. Thus, the proposed controller block can be drawn in Fig. 1.

In Fig. 1, the common bus voltage is extracted and then transferred in $\alpha\beta$-frame, which is used for establishing the pre-synchronization items in Hopf equations. On the other hand, the output current is progressed in the same way to ensure the inner-synchronization among the VSIs. Next, the voltage references generated by Hopf equations are transformed from $\alpha\beta$-frame to the abc-frame, and scaled by dc-link voltage to obtain the modulation signals. The three items in proposed equations are discussed in details as below:

1) Hopf oscillator item: This is a general sinusoidal signals generation part to follow the voltage and frequency references. The orthogonal voltage references should be ensured through the bifurcations theory.

2) Pre-synchronization item: Although the oscillatorcontrolled inverters system has synchronization property, the dynamics are able to occur undesirable overshoot when inverters connect. In classical droop controller, PLL should be added to guarantee the pre-synchronization. However, extra PLL controller will limit the control bandwidth and increase the complexity of system design. In proposed method, the voltage pre-synchronization item is used for synchronizing with common bus voltage automatically through nonlinear oscillator property. Before the breaker action, each VSI can synchronize with AC bus, which can facilitate the unwanted addition overshoot with desired transients. Note that this item is no required to switch extra synchronization blocks, which is

convenient to control in practice.

3) Current sharing item: The coupling between oscillators is realized through this item. As the current information is able to flow in both directions, the current sharing item results in the possibility of synchronization among oscillator controllers. At a word, this item ensures the inner synchronization to realize current sharing, and the k_i scales the output current to vary the current sharing ratio.

B. Averaged Model

Since the controller equation is nonlinear based on time domain, the regular frequency domain analysis method is difficult to observe the dynamics. However, the averaged model is an effective way to analyze the nonlinear system in steady state. Consider the time-varying dynamical system $\dot{x} = f(x, t, \varepsilon)$ with small parameter ε. The average model is given by:

$$\dot{x} = \varepsilon f_{av}(x) = \frac{\varepsilon}{T}\int_0^T f(x, t, 0)\mathrm{d}t \tag{2}$$

For an oscillator system, it has an stable T-periodic solution in an region $O(\varepsilon)$ of equilibrium. The the difference between the initial state and average can be defined as:

$$O(\varepsilon) = x(t, \varepsilon) - \bar{x}(\varepsilon t),\ \forall\, t \geqslant 0 \tag{3}$$

In order to standard perturbation and proceed to approximate the periodic solution, the variables can be changed into y. The T-periodic solution of original system can be given by [20]:

$$x = y + \varepsilon\int_0^T [f(t, y, 0) - f_{av}(y)]\mathrm{d}t \tag{4}$$

According to (4), how the solution of the averaged model averages the actual system is able to be obtained. Subsequently, for the averaged solution of system can be defined as:

$$\bar{x} = \frac{1}{T}\int_0^T x(t)\mathrm{d}t \tag{5}$$

Fig. 2 presents the limit cycle comparison of the exact and averaged solution in steady state. Based on the preliminaries model, the voltage-active power and frequency-reactive power characteristics will be derived as follows. By differentiating $V_\alpha = V\sin(\theta)$, $V_\beta = V\cos(\theta)$ with respect to time, there are:

$$\begin{cases} \dot{V}_\alpha = \sin(\theta)\dot{V} + V\cos(\theta)\dot{\theta} \\ \dot{V}_\beta = \cos(\theta)\dot{V} - V\sin(\theta)\dot{\theta} \end{cases} \tag{6}$$

where θ is the instantaneous phase angle of inverter output. Because the common bus voltage is approximately equal to inverter terminal output voltage when filter and line impedance are small, assume $V_{c\alpha} \approx V_\alpha$ and $V_{c\beta} \approx V_\beta$. Substituting (6) to (1), the phase dynamics equations of Hopf oscillator is obtained as follows:

$$\begin{cases} \dot{V} = \mu(|V_{\mathrm{ref}}|^2 V - V^3) + k_v V - k_i[i_\alpha\cos(\theta) + i_\beta\sin(\theta)] \\ \dot{\theta} = \omega + \dfrac{k_i}{V}[i_\alpha\sin(\theta) - i_\beta\cos(\theta)] \end{cases} \tag{7}$$

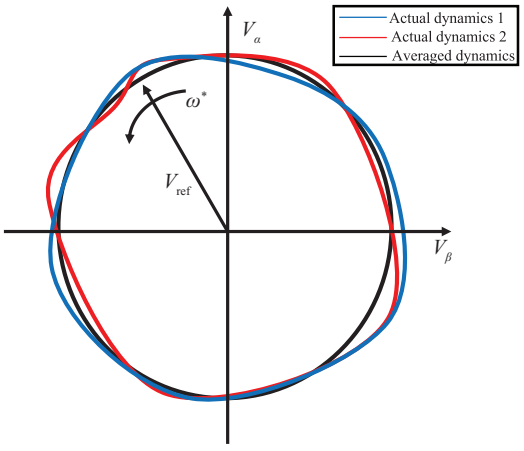

Fig. 2. The steady-state limit cycles corresponding to the actual and averaged oscillator dynamics.

For simplifying the averaged model, the dynamics of the inverter terminal voltage is expressed as:

$$\frac{\mathrm{d}\theta}{\mathrm{d}t} = \omega + \frac{\mathrm{d}\varphi}{\mathrm{d}t} = \omega^* + \frac{\mathrm{d}\varphi^*}{\mathrm{d}t} \tag{8}$$

where ω and ω^* are the nominal frequency of inverter output, and the steady state frequency of inverter output, respectively. The angels φ and φ^* are the phase offset with respect to ω and ω^*, respectively. Thus, the Hopf oscillator dynamical system in 2π-periodic function are derived as:

$$\begin{cases} \dot{\bar{V}} = \dfrac{\omega^*}{2\pi}\displaystyle\int_0^{\frac{2\pi}{\omega^*}}\left[\mu(|V_{\mathrm{ref}}|^2 V - V^3) + k_v V\right]\mathrm{d}t \\ \qquad -\dfrac{\omega^* k_i}{2\pi}\displaystyle\int_0^{\frac{2\pi}{\omega^*}} i_\alpha\cos(\omega^* t + \varphi^*) + i_\beta\sin(\omega^* t + \varphi^*)\mathrm{d}t \\ \dot{\bar{\varphi}}^* = \dfrac{\omega^* k_i}{2\pi V}\displaystyle\int_0^{\frac{2\pi}{\omega^*}} i_\alpha[\sin(\omega^* t + \varphi^*) - i_\beta\cos(\omega^* t + \varphi^*)]\mathrm{d}t \end{cases} \tag{9}$$

Considering the perturbation i_α, i_β, which are related to the instantaneous power P, Q. The definition and average equations during 2π-period of $\bar{P}$ and $\bar{Q}$ are shown as:

$$\begin{cases} P(t) = \dfrac{3}{2}(V_\alpha i_\alpha + V_\beta i_\beta) \\ Q(t) = \dfrac{3}{2}(V_\beta i_\alpha - V_\alpha i_\beta) \end{cases}, \begin{cases} \bar{P} = \dfrac{\omega^*}{2\pi}\displaystyle\int_0^{2\pi/\omega^*} P(t)\mathrm{d}t \\ \bar{Q} = \dfrac{\omega^*}{2\pi}\displaystyle\int_0^{2\pi/\omega^*} Q(t)\mathrm{d}t \end{cases} \tag{10}$$

Substituting (10) to (9), (9) can be rewritten as:

$$\begin{bmatrix} \dot{\bar{V}} \\ \dot{\bar{\varphi}}^* \end{bmatrix} = \begin{bmatrix} \mu|V_{\mathrm{ref}}|^2\bar{V} - \mu\bar{V}^3 + k_v\bar{V} \\ 0 \end{bmatrix} + \begin{bmatrix} -\dfrac{2k}{3\bar{V}}\bar{P} \\ \dfrac{2k}{3\bar{V}^2}\bar{Q} \end{bmatrix} \tag{11}$$

Based on (11) and (8), the amplitude and phase dynamics of

one oscillator are derived as:

$$\begin{cases} \dot{\bar{V}} = \left|V_{\text{ref}}\right|^2 \mu \bar{V} - \bar{V}^3 \mu + k_v \bar{V} - \dfrac{2k_i}{3\bar{V}} \bar{P} \\ \dot{\bar{\theta}} = \omega^* - \omega + \dfrac{2k_i}{3\bar{V}^2} \bar{Q} \end{cases} \tag{12}$$

Similar to droop control, the $V-P$ and $\theta-Q$ relationship are derived. Note that dynamics of amplitude and phase for Hopf oscillator controller is nonlinear that is different from the linear relationship of conventional droop controller. However, the oscillator controller does not require the power measurement or low pass filter during operation. The interesting part is the averaged model of oscillator processing corresponds to the low pass filter for power in droop.

C. Parameter Selection

The design of scaling factor k_v and k_i are the primarily part for the proposed controller. The characteristic equations of (12) are:

$$\begin{cases} \left|V_{\text{ref}}\right|^2 \mu \bar{V}_{\text{eq}} - \bar{V}_{\text{eq}}^3 \mu + k_v \bar{V}_{\text{eq}} - \dfrac{2k_i}{3\bar{V}_{\text{eq}}} \bar{P}_{\text{eq}} = 0 \\ \omega^* + \dfrac{2k_i}{3\bar{V}_{\text{eq}}^2} \bar{Q}_{\text{eq}} = \omega_{\text{eq}} \end{cases} \tag{13}$$

where symbol subscript eq refers to the equilibrium in steady sate. The positive roots of amplitude equation in (13) are solved as:

$$\bar{V}_{\text{eq}} = \sqrt{0.5\mu\left(k_v^2 \pm \sqrt{\left(\left|V_{\text{ref}}\right|^2 \mu + k_v\right)^2 - \frac{8}{3}\mu k_i \bar{P}_{\text{eq}}} + \mu\left|V_{\text{ref}}\right|^2\right)} \tag{14}$$

When the oscillator operates in open loop, the corresponding critical values $\bar{V}_{\text{eqmin}}$ and $\bar{V}_{\text{eqmax}}$ of the output voltage is:

$$\bar{V}_{\text{eqmin}} := 0 < \bar{V} < \bar{V}_{\text{eqmax}} := \sqrt{\left|V_{\text{ref}}\right|^2 + \frac{k_v}{\mu}} \tag{15}$$

Subsequently, to make sure the roots are real in (13) , the critical value of active power $\bar{P}_{\text{eqmax}}$ is given by:

$$0 < \bar{P} < \bar{P}_{\text{eqmax}} := \frac{3\left(k_v + \mu\left|V_{\text{ref}}\right|^2\right)^2}{8\mu k_i} \tag{16}$$

Therefore, assume that $\bar{P}_{\text{eqmax}} = \bar{P}_{\text{rated}}$. Otherwise, the rated reactive $\bar{Q}_{\text{rated}}$ and rated voltage $\bar{V}_{\text{rated}}$ are regarded as inputs. Define the maximum frequency deviation as $\Delta\omega_{\max}$. Accordingly, the k_i operation range satisfies as follows:

$$k_i \leqslant \frac{3\Delta\omega_{\max} \bar{V}_{\text{rated}}^2}{2\bar{Q}_{\text{rated}}} \tag{17}$$

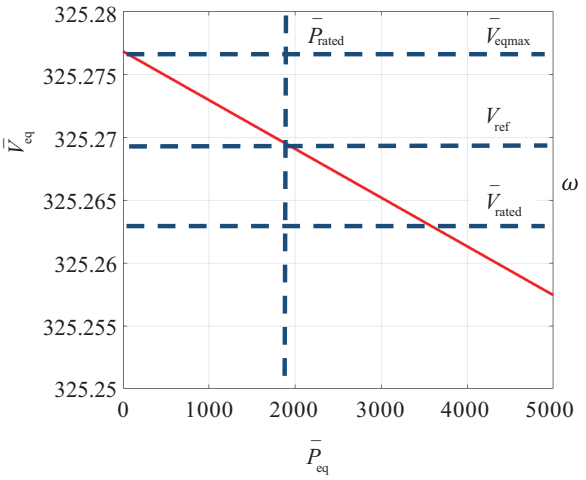

(a)

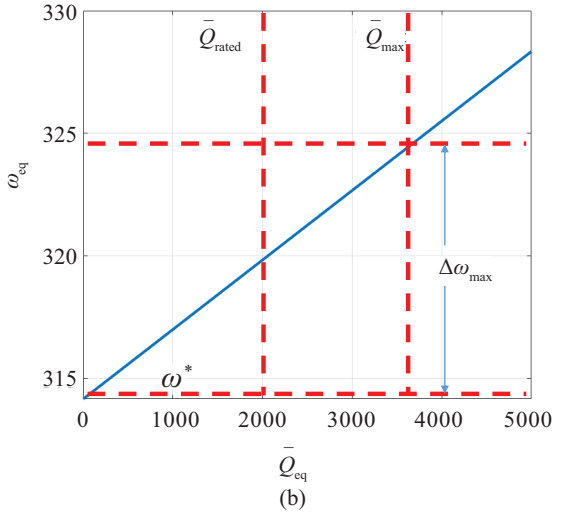

(b)

Fig. 3. The droop and ascend characteristics for (a) $\bar{V}_{\text{eq}} - \bar{P}_{\text{eq}}$, (b) $\bar{\omega}_{\text{eq}} - \bar{Q}_{\text{eq}}$.

In order to standardize parameters, select the k_i when the Prated output current is 1 A, so the current gain is $\bar{P}_{\text{rated}}/\bar{V}_{\text{rated}}$. Therefore, Vrated based on (17) and (16), the maximum value of k_v is able to be expressed as:

$$k_v \leqslant \frac{2\Delta\omega_{\max} \bar{V}_{\text{rated}}^2 \sqrt{\mu \bar{V}_{\text{rated}}}}{\bar{Q}_{\text{rated}}} - \mu\left|V_{\text{ref}}\right|^2 \tag{18}$$

For observing the equilibrium voltage and phase characteristics, Fig. 3 shows the droop and ascend diagram for $\bar{V}_{\text{eq}} - \bar{P}$ and $\bar{\omega}_{\text{eq}} - \bar{Q}$ based on (13) and (14). The operation parameters are $k_v = 5$, $\mu = 1$, $k_i = 1000$, $\omega = 100\pi$ rad/s, and $|V_{\text{ref}}| = 325.27$ V . In Fig. 3 (a), a droop law between equilibrium voltage and equilibrium active power appears, which is familiar to conventional droop laws there exists voltage variation when the active power changes. However, in Fig. 3(b), unlike droop control, the relationship between frequency and equilibrium reactive power presents ascend laws, which means equilibrium frequency in time-domain increases to infinity when reactive

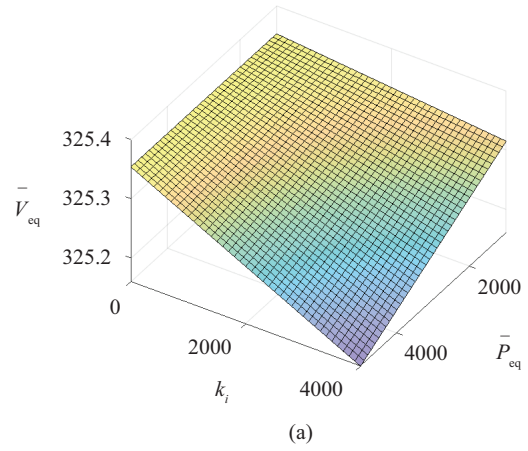

(a)

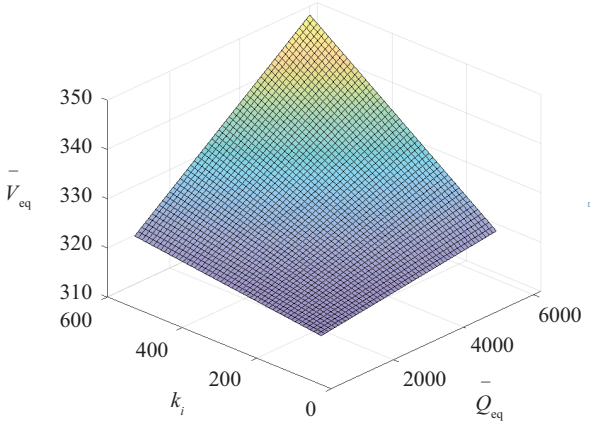

(b)

Fig. 4. (a) The relationship between k_i and the equilibrium voltage amplitude and active power. (b) The relationship between k_i and the equilibrium voltage amplitude and reactive power .

power increase. Thus, the maximum frequency offset should regulate the frequency variation.

Furthermore, Fig. 4(a) and (b) illustrate the voltage is reduced with respect to k_i and $\bar{P}_{eq}$, and increased with respect to k_i and $\bar{Q}_{eq}$. k_i affects the ratios value of the droop and ascend laws for Hopf-oscillator controller. It can be seen that k_i is an insensitive parameter to compare with conventional droop controller, which also implies the solid and steady characteristics of the nonlinear droop. On the other hand, a large range of k_v varying will not change the voltage amplitude in Fig. 5, and k_v only has impacts on the pre-synchronization speed and critical of voltage equilibrium.

III. Stability Analyses for Hopf Oscillator-Controlled Islanded System

Aiming to obtain precise matching between steady-state model and simulation in time domain, a flexible small signal model is built in this part where Fig. 6 shows the two paralleled VSIs connect to the common AC bus through line impedance. Define V_{1dq}, i_{1dq}, V_{2dq}, and i_{2dq} as the voltage amplitude and output current of VSI #1 and #2 in rotating frame, respectively, and

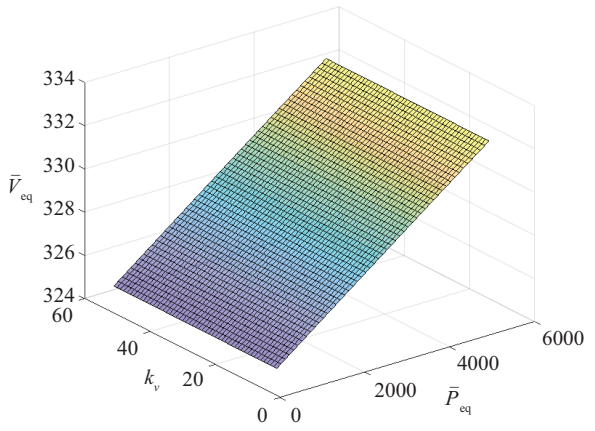

Fig. 5. The relationship between k_v and the equilibrium voltage amplitude and active power.

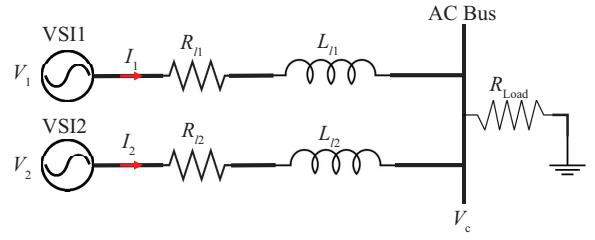

Fig. 6. Equivalent circuit of two VSIs connect to the common AC bus with resistive load.

define V_1, P_1, Q_1 θ_1 and V_2, P_2, Q_2 θ_2 as the voltage amplitude, output active power, output reactive power, and phase of VSI #1 and #2, respectively. Set the voltage of VSI #1 as the reference, so there are $V_{1d} = V_1$, $V_{1q} = 0$ and $V_2 = \sqrt{V_{2d}^2 + V_{2q}^2}$. Based on the definition before, the output active power of VSI #1 and #2 are given as:

$$\begin{cases} P_1 = \dfrac{3}{2} V_{1d} i_{1d},\ P_2 = \dfrac{3}{2}(V_{2d} i_{2d} + V_{2q} i_{2q}) \\ Q_1 = -\dfrac{3}{2} V_{1d} i_{1q},\ Q_2 = \dfrac{3}{2}(V_{2q} i_{2d} - V_{2d} i_{2q}) \end{cases} \tag{19}$$

In steady state, considering the line impedance for VSI #1 and #2, rewrite (12) as:

$$\begin{cases} \dot{V}_1 = f_1 = \left| V_{\text{ref}} \right|^2 \mu V_c - V_1^3 \mu + k_v V_1 - \dfrac{2k_i}{3V_1} P_1 \\ \dot{V}_2 = f_2 = \left| V_{\text{ref}} \right|^2 \mu V_c - V_2^3 \mu + k_v V_2 - \dfrac{2k_i}{3V_2} P_2 \\ \dot{\theta}_1 = \omega^* + \dfrac{2k_i}{3V_1^2} Q_1 \\ \dot{\theta}_2 = \omega^* + \dfrac{2k_i}{3V_2^2} Q_2 \end{cases} \tag{20}$$

where V_c is the amplitude of AC bus voltage. The dynamics equations governing the line impedance of VSI #1 and #2 are

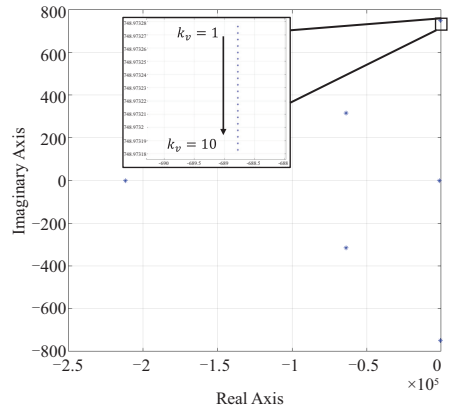

(a)

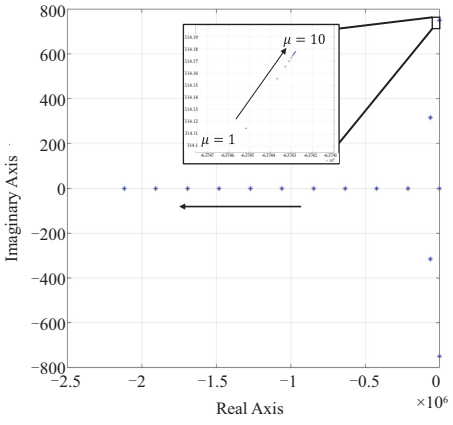

(b)

Fig. 7. Root locus diagrams for (a) $1 \leqslant k_v \leqslant 10$, (b) $1 \leqslant \mu \leqslant 10$.

expressed as:

$$\begin{cases} \dfrac{\mathrm{d}i_{1d}}{\mathrm{d}t} = f_3 = \dfrac{-R_{l1}}{L_{l1}} i_{1d} + \dot{\theta}_1 i_{1q} + \dfrac{1}{L_{l1}} v_{1d} - \dfrac{1}{L_{l1}} v_{cd} \\ \dfrac{\mathrm{d}i_{2d}}{\mathrm{d}t} = f_4 = \dfrac{-R_{l2}}{L_{l2}} i_{2d} + \dot{\theta}_2 i_{2q} + \dfrac{1}{L_{l2}} v_{2d} - \dfrac{1}{L_{l2}} v_{cq} \\ \dfrac{\mathrm{d}i_{1q}}{\mathrm{d}t} = f_5 = \dfrac{-R_{l1}}{L_{l1}} i_{1q} - \dot{\theta}_1 i_{1d} + \dfrac{1}{L_{l1}} v_{1q} - \dfrac{1}{L_{l1}} v_{cq} \\ \dfrac{\mathrm{d}i_{2q}}{\mathrm{d}t} = f_6 = \dfrac{-R_{l2}}{L_{l2}} i_{2q} - \dot{\theta}_2 i_{2d} + \dfrac{1}{L_{l2}} v_{2q} - \dfrac{1}{L_{l2}} v_{cq} \end{cases} \tag{21}$$

where v_{cd} and v_{cq} is the d and q component of common bus voltage.

Because the phase increases indefinitely as derived in (12), define the frequency error as:

$$\Delta\dot{\theta} = f_7 = \dot{\theta}_1 - \dot{\theta}_2 = \frac{2k_i}{3}\left(\frac{Q_1}{V_1^2} - \frac{Q_2}{V_2^2}\right) \tag{22}$$

Select $\Delta X = [\Delta V_1\ \Delta V_2\ \Delta\theta\ \Delta i_{1d}\ \Delta i_{1q}\ \Delta i_{2d}\ \Delta i_{2q}]$ as the state vector, and $f = [f_1\ f_2\ f_3\ f_4\ f_5\ f_6\ f_7]^{\mathrm{T}}$. According to (20)–(22), the linearized small-signal model is given by:

$$\dot{\Delta X} = A\Delta X \tag{23}$$

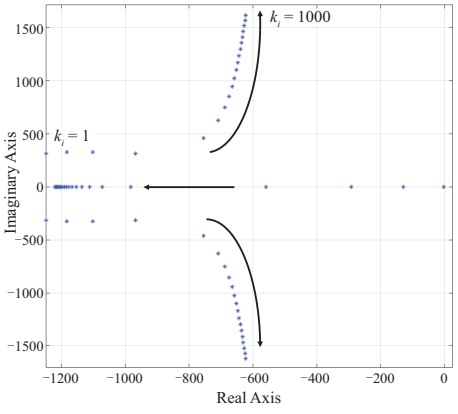

Fig. 8. Root locus diagram for $1 \leqslant k_i \leqslant 1000$.

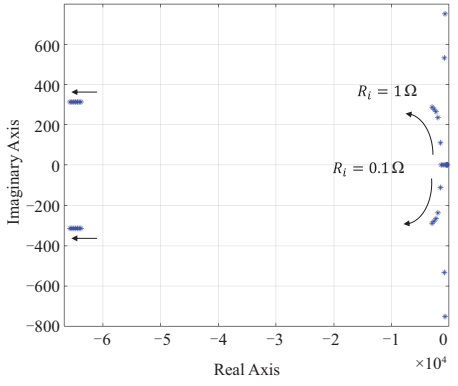

(a)

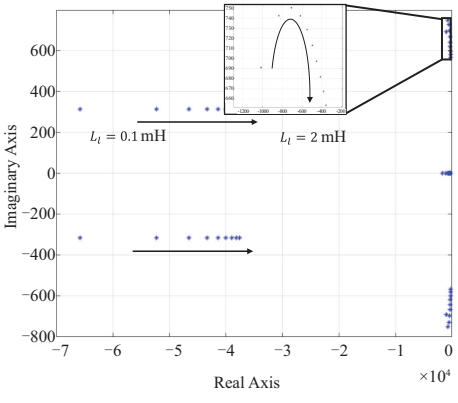

(b)

Fig. 9. Root locus diagrams for (a) $0.1\ \Omega \leqslant R_l \leqslant 1\ \Omega$, (b) $0.1\ \mathrm{mH} \leqslant L_l \leqslant 1\ \mathrm{mH}$.

where $\boldsymbol{A} = \partial f/\partial x^T$. It is clear to see that U is 7×7 square matrix with time-invariant matrices. So the eigenvalues of state matrix U are derive through [21], [22]:

$$det(s\boldsymbol{I} - \boldsymbol{A}) = 0 \tag{24}$$

The influences of parameters k_v, μ, k_i and line impedance are discussed as below. Note that the small-signal linearization model not only analyzes the input-output dynamics of the system, but also offers a global diagram for the eigenvalues responses.

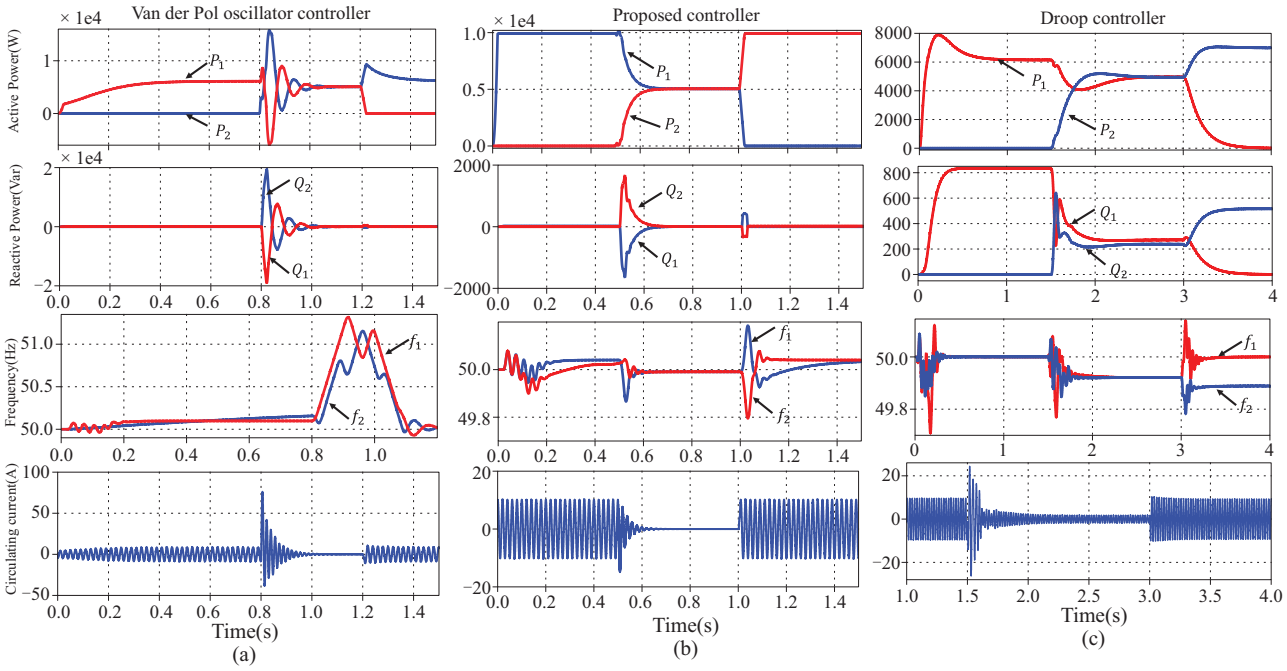

Fig. 10. Transient responses of three methods under adding and removing a inverter cases with active and reactive power, output current frequency, and circulating current.

Fig. 7 illustrate that the eigenvalues clusters intersperse in negative real dominant for both k_v and μ. When k_v and μ are increased, the modes move slightly, which means the parameters k_v and μ are insensitive to the stability of system. Fig. 8 shows k_i is sensitive to the stability of system. k_i has a largely impact on the transient response of VSI, and the damping is reducing when k_i is increasing.

At last, Fig. 9 show the trajectory of eigenvalues in terms of the line impedance R_l and L_l. It is clear to observe that there are a family of modes gather closing to the unstable region. Separately, for R_l increasing, the eigenvalues become more sensitive to the states of controller. On the other hand, for L_l increasing, the eigenvalues move towards to the unstable region and the damping of system is even less. Hence, regarding the Hopf oscillator-controlled system, k_i is the most critical parameters that has influence on the dynamics of system.

IV. Simulation Validation

The performance of the proposed method first is verified by simulation to compare with droop and VOC method. Both inverters have same DC voltage V_{dc} = 450 V, and the LCL filter values are: L_1 =1.8 mH, C = 10 μF, L_2 =1.8 mH, the voltage reference V_{ref} = 325 V, and the frequency reference $\omega = 100\pi$. For $P - f/Q - V$ droop controller, the droop coefficients are m = 0.00001, n = 0.0002. The Visual oscillator controller parameters are chosen from [17]. For the proposed controller: k_i = 300, k_v = 10. Various simulation tests for example, startup, connection, current ratio changes, nonlinear loads connection of inverters were carried out.

Fig. 10. shows the transient response of output current and active power with the scenario of VSI #1 startup and VSI #2 connection and removal in the presence of a resistive load 100 Ω. As seen in Fig. 10(a), the Van der Pol oscillator controller has approximately 0.5 s starting time, and the settling time is 0.18 s when VSI #2 connects. Note that the initial conditions of Van der Pol oscillators were selected to be 3 V considering emulating errors. For droop controller, the starting time is faster with slight overshoot. But the settling time is much longer than VOC with 0.75 s. Note that the frequency deviation is much larger with error 0.06 Hz in Fig. 10(c). In comparison, as shown in Fig. 10(b), the starting time of the Hopf oscillator controller is approximately 0.02 s with (0 V, 0 V) initial conditions. The proposed controller is able to realize power sharing and the settling time of connection is approximately 0.11 s. It is clear to observe that the Hopf oscillator reahces steady state faster than other two methods in case of startup , connection and removal.

The transient response for sudden direct currents ratio changes of parallel VSIs with three control strategies are illustrated in Fig. 11. The current ratio has been suddenly changed from 1:1 to 2:1. It can be observed that the current outputs of three control methods are nearly instantaneous from 1:1 to 2:1. Note that the transient response of Hopf oscillator controller lasts 0.15 s compared with 0.21 s of the Van der Pol, and 0.18 of the droop. It is worthy to observe that the phase error appears because the Q, f characteristics changing in Fig. 11(b). Additionally, a small active power overshoot occurs in waveform of the Van der Pol oscillator as shown in Fig. 11(a).

System responses to steping loads are illustrated in Fig. 12. At 0.6 s, the resistive load is changed from 100 Ω to 200 Ω. At 1.2 s, resistive load is changed to a diode bridge rectifier load (200 Ω + 100 μF). Notice that the load current of three oscillator controllers increase abruptly, and the load voltage continues to meet specifications. It is worth noting that there are a overshoot for oscillators controller when nonlinear loads connection, because the voltage on filter capacitor surge.

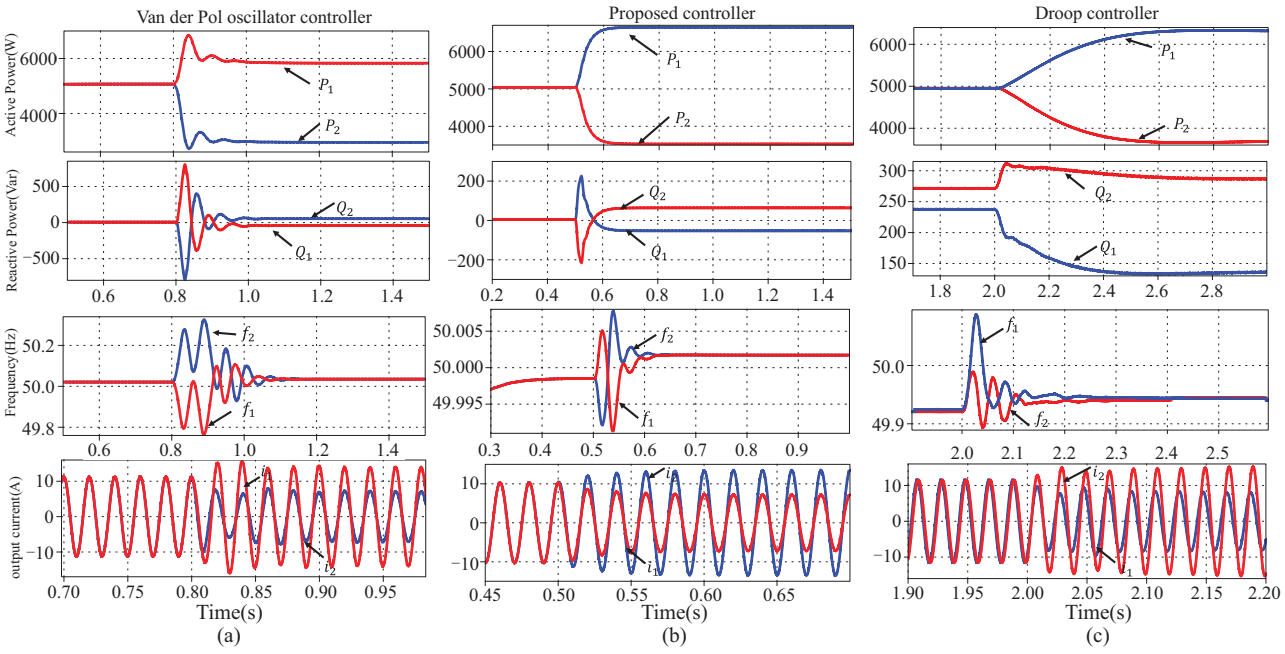

Fig. 11. Transient responses of three methods under current ratio changing from 1:1 to 2:1 with active and reactive power, output current frequency and output current.

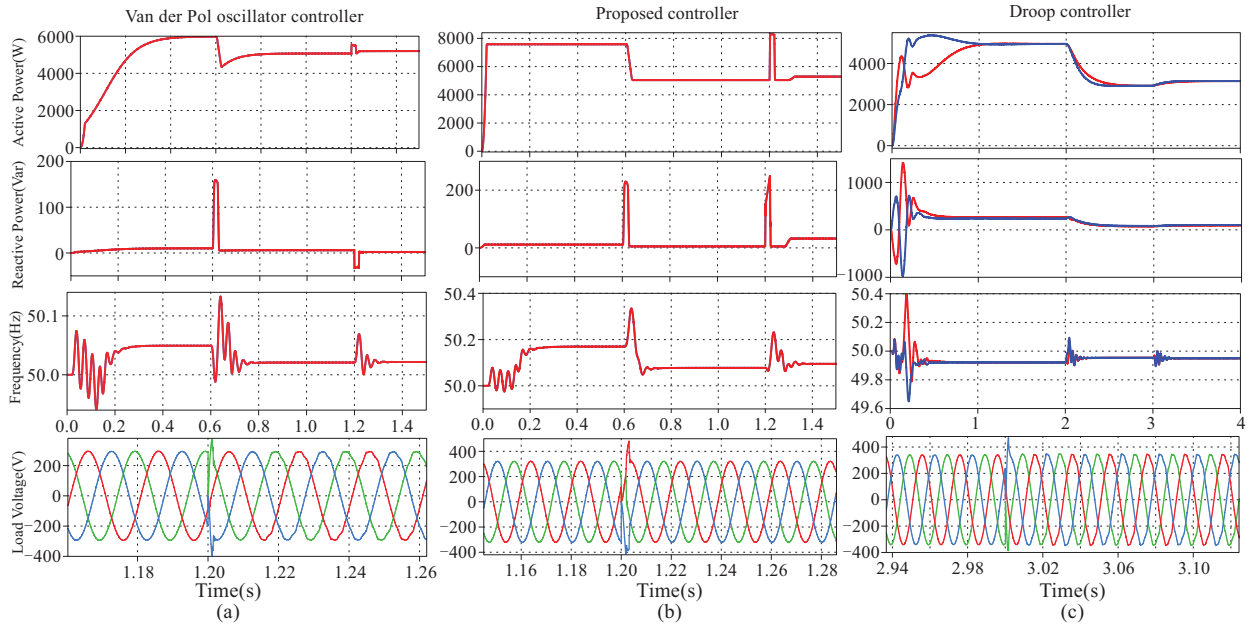

Fig. 12. Transient responses of three methods under resistive and nonlinear loads step with active and reactive power, output current frequency, and load voltage.

The power factor after 1.2 s continues to coincide as before. The load voltage THD of Van der Pol, Hopf and droop are 2.767%, 2.262% and 3.142%, respectively. Therefore, the Van der Pol and Hopf methods are proven to more valid than droop controller in the presence a nonlinear load, and the Hopf method obtains a better power quality.

V. Experiment Results

The performance of proposed controller was also validated in experimental platform, where the setup consists of two parallel three-phase Danfoss 2.2 kW inverters, LCL filters, DC voltage supply source, and the resistive load as shown in Fig. 13. The controller was implemented by the dSPACE 1006 real-time system. The switching frequency is set to 10 kHz. The setup and controller parameters are listed in Table I.

1) Inverters Connection

Above all, the transient response of instantaneous active and reactive power, output current and load voltage for sudden inverter #2 connection are shown in Fig. 14(a)–(c). The initial state of each oscillator was set to ($0.5V_{rated}$, 0) It can be observed that the settling time is much shorter than simulation

Fig. 13. Experimental setup in the laboratory.

TABLE I
THREE-PHASE PARALLEL SYSTEM PARAMETERS USED IN EXPERIMENT

Parameter	Value	Unit
DC voltage	500	V
Rated Power	2.2	kW
VSI-side Filter inductance	1.8	mH
Load-side Filter inductance	1.8	mH
Filter capacitance	25	μF
Resistive load	100	Ω
Step-up load	100	Ω
Oscillator initial state	155,0	V,V
Startup k_i	300	A/A
Startup k_v	10	V/V
Damping Coefficient μ	1	$V^{-2}s^{-1}$
Voltage reference	325	V
Frequency reference	50	Hz

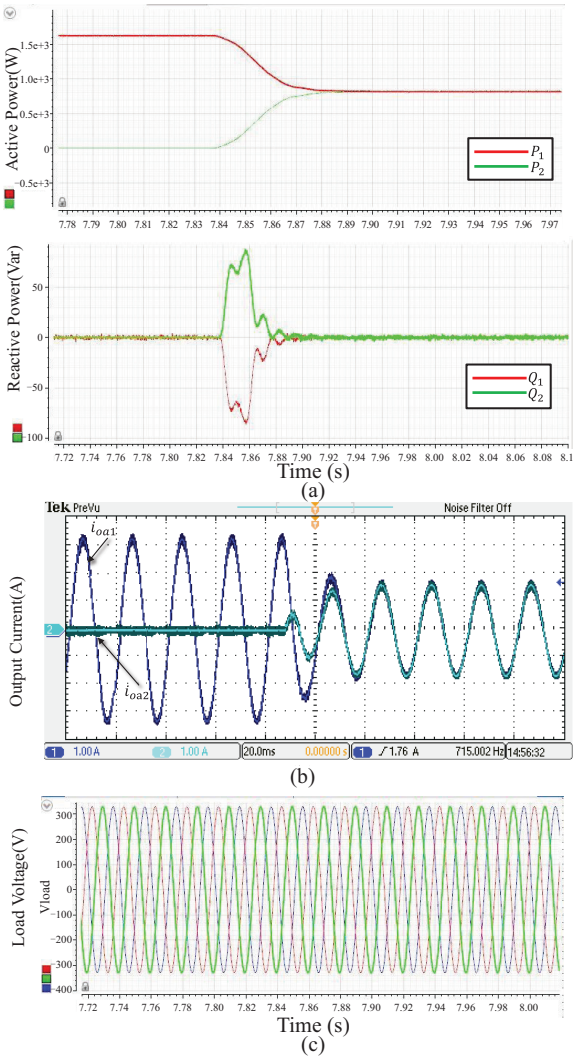

Fig. 14. Transient response of inverter connection. (a) Instantaneous active and reactive power. (b) Output current of inverter #1 and #2. (c) Load voltage.

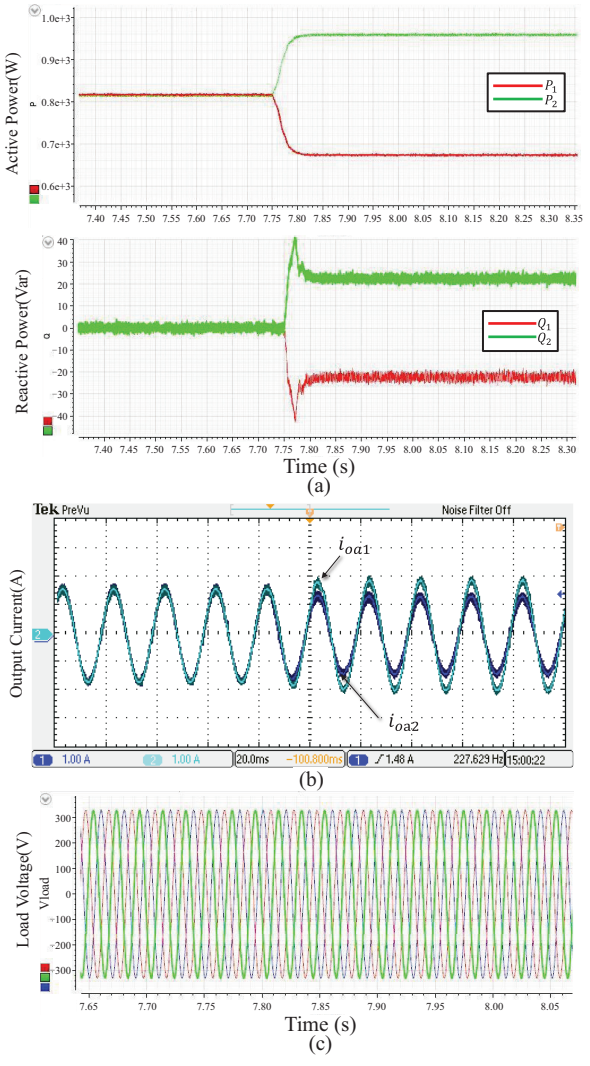

Fig. 15. Transient response of ratio changes from 1:1 to 4:3. (a) Instantaneous active and reactive power. (b) Output current of inverter #1 and #2. (c) Load voltage.

with 0.06 s, because the practical switching frequency is larger the sampling frequency without time consuming iterations.

Due to the pre-synchronization included, there is no overshoot even through the phase mismatch existing before connection. Additionally, the current transient also presents the suddenly

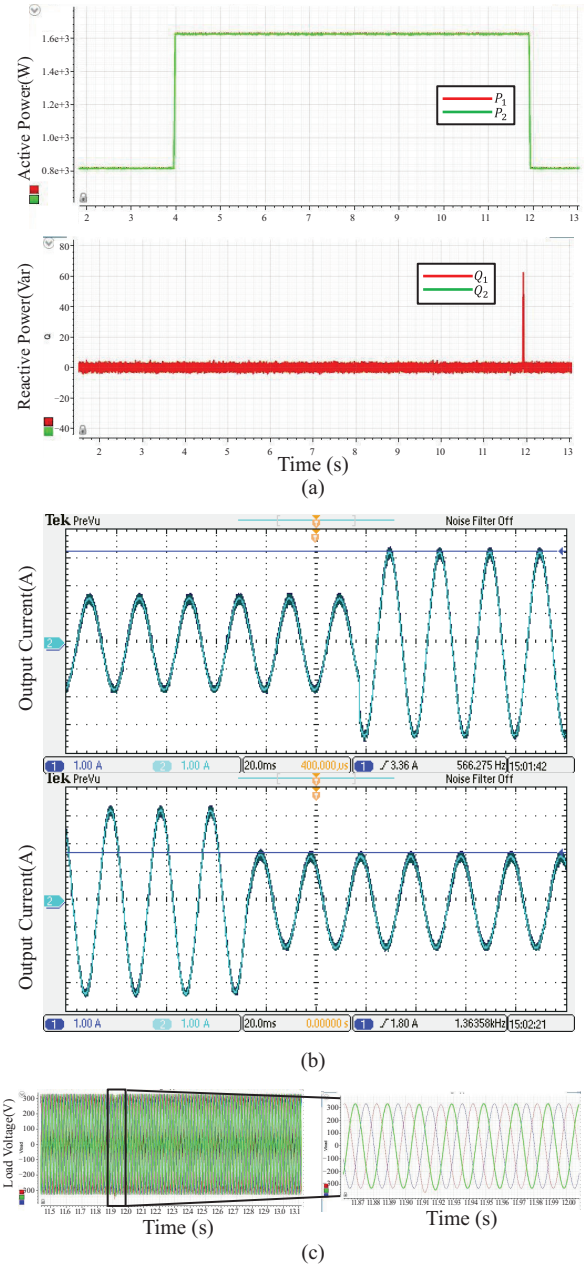

Fig. 16. Transient response of load step and inverter removal. (a) Instantaneous active and reactive power. (b) Output current of inverter #1 and #2. (c) Load voltage.

synchronizing dynamics, and the load voltage keeps stable in Fig. 14(b) and (c).

2) Ratio Changes

Incoming, Fig. 15(a)–(c) depict the transient response to k_i changes from 1:1 to 4:3. Note that the active power of each inverter separate at sudden changes, and reactive power present a small overshoot/undershoot in a short time. Then, the output currents of VSI suit their ratio nearly instantaneously as shown in Fig. 15(b), and the voltage of load also stay stable which meets the requirement of islanded Microgrid in Fig. 15(c).

3) Load steps

Fig. 16(a)–(c) show the transient response during load step twice when the two VSIs supply the resistive loads. At 4.0 s and 12.0 s, 100 Ω resistive load adds in parallel and then switch back. It can be observed that the increase and decrease dynamics of output currents are momentary in Fig. 16(b). Note that there is a obvious transient of load voltage, and it recover quickly to references.

In summary, the experimental results present that the proposed Hopf-oscillator controller can realize the pre-synchronization and current sharing in decentralized system operation. It mainly demonstrates the fast dynamics response speed and stable operation with load step.

VI. Conclusions

This paper presented a simple and fast synchronization method based on coupled Hopf-oscillators for grid-forming inverters in Microgrid. The Hopf oscillator dynamic equations were used for providing the inverter's frequency and amplitude voltage references which lead to a robust nonlinear droop behavior for driving the system without using communications. To overcome the undesired overshoot when inverters connection, the pre-synchronization item was introduced into control equations. The current sharing item was designed for inner synchronization between inverters. The $P-V$ and $Q-\omega$ relationship nonlinear droop and ascend characteristics were derived by the averaged model. Steady-state model analyses clarified the system stability performance, the relationship between the parameters and system performance. A series of comparison simulations and experiments were carried out to validate the proposed strategy. The obtained results didn't not require the power calculation and PLL, and present fast and precise synchronization and current sharing performance.

References

[1] J. Rocabert, A. Luna, F. Blaabjerg, and P. Rodriguez, "Control of power converters in AC microgrids," in *IEEE transactions on Power Electronics*, vol. 27, no. 11, pp. 4734–4749, Nov. 2012.

[2] J. M. Guerrero, P. C. Loh, T. -L. Lee, and M. Chandorkar, "Advanced control architectures for intelligent microgrids—part II: Power quality, energy storage, and AC/DC microgrids," in *IEEE Transactions on Industrial Electronics*, vol. 60, no. 4, pp. 1263–1270, Apr. 2013.

[3] K. De Brabandere, B. Bolsens, J. Van den Keybus, A. Woyte, J. Driesen, and R. Belmans, "A voltage and frequency droop control method for parallel inverters," in *IEEE Transactions on Power Electronics*, vol. 22, no. 4, pp. 1107–1115, Jul. 2007.

[4] E. Barklund, N. Pogaku, M. Prodanovic, C. Hernandez-Aramburo, and T. C. Green, "Energy management in autonomous microgrid using stability-constrained droop control of inverters," in *IEEE Transactions on Power Electronics*, vol. 23, no. 5, pp. 2346–2352, Sept. 2008.

[5] J. Liu, Y. Miura, and T. Ise, "Comparison of dynamic characteristics between virtual synchronous generator and droop control in inverter-based distributed generators," in *IEEE Transactions on Power Electronics*, vol. 31, no. 5, pp. 3600–3611, May 2016.

[6] H. Bevrani and S. Shokoohi, "An intelligent droop control for simultaneous voltage and frequency regulation in islanded microgrids," in *IEEE Transactions on Smart Grid*, vol. 4, no. 3, pp. 1505–1513, Sept. 2013.

[7] Y. Li and Y. W. Li, "Decoupled power control for an inverter based low voltage microgrid in autonomous operation," in *2009 IEEE 6th International Power Electronics and Motion Control Conference*, Wuhan, China, 2009, pp. 2490–2496.

[8] T. Wu, Z. Liu, J. Liu, S. Wang, and Z. You, "A unified virtual power decoupling method for droop-controlled parallel inverters in microgrids," in *IEEE Transactions on Power Electronics*, vol. 31, no. 8, pp. 5587–

5603, Aug. 2016.
[9] M. Ashabani, A. -R. M. Yasser, M. Mirsalim, and M. Aghashabani, "Multivariable droop control of synchronous current converters in weak grids/microgrids with decoupled dq-axes currents," in *IEEE Transactions on Smart Grid*, vol. 6, no. 4, pp. 1610–1620, Jul. 2015.
[10] J. He, Y. W. Li, J. M. Guerrero, F. Blaabjerg, and J. C. Vasquez, "An islanding microgrid power sharing approach using enhanced virtual impedance control scheme," in *IEEE Transactions on Power Electronics*, vol. 28, no. 11, pp. 5272–5282, Nov. 2013.
[11] J. Matas, M. Castilla, L. G. De Vicuña, J. Miret, and J. C. Vasquez, "Virtual impedance loop for droop-controlled single-phase parallel inverters using a second-order general-integrator scheme," in *IEEE Transactions on Power Electronics*, vol. 25, no. 12, pp. 2993–3002, Dec. 2010.
[12] A. Micallef, M. Apap, C. Spiteri-Staines, J. M. Guerrero, and J. C. Vasquez, "Reactive power sharing and voltage harmonic distortion compensation of droop controlled single phase islanded microgrids," in *IEEE Transactions on Smart Grid*, vol. 5, no. 3, pp. 1149–1158, May 2014.
[13] H. Han, Y. Liu, Y. Sun, M. Su, and J. M. Guerrero, "An improved droop control strategy for reactive power sharing in islanded microgrid," in *IEEE Transactions on Power Electronics*, vol. 30, no. 6, pp. 3133–3141, Jun. 2015.
[14] Y. Guan, J. M. Guerrero, X. Zhao, J. C. Vasquez, and X. Guo, "A new way of controlling parallel-connected inverters by using synchronous-reference-frame virtual impedance loop—part I: Control principle," in *IEEE Transactions on Power Electronics*, vol. 31, no. 6, pp. 4576–4593, Jun. 2016.
[15] B. B. Johnson, S. V. Dhople, A. O. Hamadeh, and P. T. Krein, "Synchronization of parallel single-phase inverters with virtual oscillator control," in *IEEE Transactions on Power Electronics*, vol. 29, no. 11, pp. 6124–6138, Nov. 2014.
[16] B. B. Johnson, S. V. Dhople, A. O. Hamadeh, and P. T. Krein, "Synchronization of nonlinear oscillators in an lti electrical power network," in *IEEE Transactions on Circuits and Systems I: Regular Papers*, vol. 61, no. 3, pp. 834–844, Mar. 2014.
[17] B. B. Johnson, S. V. Dhople, J. L. Cale, A. O. Hamadeh, and P. T. Krein, "Oscillator-based inverter control for islanded three-phase microgrids," in *IEEE Journal of Photovoltaics*, vol. 4, no. 1, pp. 387–395, Jan. 2014.
[18] B. B. Johnson, M. Sinha, N. G. Ainsworth, F. Dörfler, and S. V. Dhople, "Synthesizing virtual oscillators to control islanded inverters," in *IEEE Transactions on Power Electronics*, vol. 31, no. 8, pp. 6002–6015, Aug. 2016.
[19] M. Li, Y. Gui, Y. Guan, J. Matas, J. M. Guerrero, and J. C. Vasquez, "Inverter parallelization for an islanded microgrid using the Hopf oscillator controller approach with self-synchronization capabilities," in *IEEE Transactions on Industrial Electronics*, under review.
[20] H. K. Khalil and J. W. Grizzle, "Nonlinear systems," vol. 3, NJ: Prentice Hall Upper Saddle River, 2002.
[21] X. Guo, Z. Lu, B. Wang, X. Sun, L. Wang, and J. M. Guerrero, "Dynamic phasors-based modeling and stability analysis of droop-controlled inverters for microgrid applications," in *IEEE Transactions on Smart Grid*, vol. 5, no. 6, pp. 2980–2987, Nov. 2014.
[22] H. Liang, B. J. Choi, W. Zhuang, and X. Shen, "Stability enhancement of decentralized inverter control through wireless communications in microgrids," in *IEEE Transactions on Smart Grid*, vol. 4, no. 1, pp. 321–331, Mar. 2013.

Mingshen Li received the B.S. degree in electrical engineering from Chongqing University, Chongqing, China, in 2013, and the M.S. degree from the College of Electrical and Information Engineering, Hunan University, Changsha, China, in 2016. He is currently pursuing the Ph.D. degree with the Department of Energy Technology, Aalborg University, Aalborg, Denmark.

His current research interests include primary control of converters, microgrid cluster systems, and distributed generation systems.

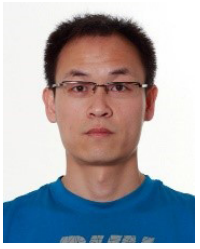

Baoze Wei received the B.S. degree in electrical engineering, the M.S. degree in power electronics and power drives from Yanshan University, Qinhuangdao, China, and the Ph.D. degree in power electronic systems from the Department of Energy Technology, Aalborg University, Aalborg, Denmark, in 2010, 2014, and 2017, respectively. He is currently working in the Department of Energy Technology, Aalborg University as an assistant professor.

His research interests include AC, DC microgrids, microgrid clusters, modular power inverters for uninterruptible power system, photovoltaic generation system, paralleling power converter for renewable generation systems, power quality, as well as the applications of distributed control.

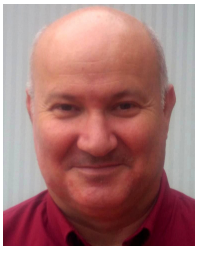

Jose Matas received the B.S., M.S., and Ph.D. degrees in telecommunications engineering from the Technical University of Catalonia, Barcelona, Spain, in 1988, 1996, and 2003, respectively. From 1988 to 1990, he was an Engineer with a consumer electronics company. Since 1990, he has been an Associate Professor with the Department of Electronic Engineering, Technical University of Catalonia, Spain. In 2017, he enrolled to the Department of Electrical Engineering. His research interests include the areas of power electronics, nonlinear control, power quality, renewable energy systems, smart grid, and microgrids.

Josep Maria Guerrero received the B.S. degree in telecommunications engineering, the M.S. degree in electronics engineering, and the Ph.D. degree in power electronics from the Technical University of Catalonia, Barcelona, Spain, in 1997, 2000, and 2003, respectively.

Since 2011, he has been a Full Professor with the Department of Energy Technology, Aalborg University, Aalborg, Denmark, where he is respon-sible for the Microgrid Research Program (www.microgrids.et.aau.dk). His research interest focuses on different microgrid aspects.

Dr. Guerrero was the recipient of the best paper award of the *Journal of Power Electronics* in 2016. In 2014, 2015, 2016, and 2017, he was awarded by T. Reuters as Highly Cited Researcher, and in 2015, he was elevated as the IEEE Fellow for his contributions on distributed power systems and microgrids.

Juan Carlos Vasquez received the B.S. degree in electronics engineering from Universidad Autnoma de Manizales, Manizales, Colombia, in 2004, and the Ph.D. degree in automatic control, robotics, and computer vision from the Technical University of Catalonia, Barcelona, Spain, in 2009.

In 2011, he was an Assistant Professor with the Department of Energy Technology, Aalborg University, Aalborg, Denmark. Since 2018, he has been an Professor with the Department of Energy Technology, Aalborg University, where he is the Vice Programme Leader of the Microgrids Research Program. His current research interests include operation, advanced hierarchical and cooperative control, and the integration of Internet of Things into the Smart Grid.

Dr. Vasquez is an Associate Editor for the *IET Power Electronics*. In 2017, he was awarded by Thomson Reuters as a Highly Cited Researcher. He is currently a member of the IECSEG4 on LVDC safety for use in developed and developing economies, the TC-RES in the IEEE Industrial Electronics, PELS, IAS, and PES Societies.